

# Construction of Hamiltonians by machine learning of energy and entanglement spectra

Hiroyuki Fujita,<sup>1,\*</sup> Yuya O. Nakagawa,<sup>1</sup> Sho Sugiura,<sup>1</sup> and Masaki Oshikawa<sup>1</sup>

<sup>1</sup>*Institute for Solid State Physics, The University of Tokyo. Kashiwa, Chiba 277-8581, Japan*

(Dated: July 13, 2022)

Correlated many-body problems ubiquitously appear in various fields of physics such as condensed matter physics, nuclear physics, and statistical physics. However, due to the interplay of the large number of degrees of freedom, it is generically impossible to treat these problems from first principles. Thus the construction of a proper model, namely effective Hamiltonian, is essential. Here, we propose a simple scheme of constructing Hamiltonians from given energy or entanglement spectra with machine learning. Taking the Hubbard model at the half-filling as an example, we show that we can optimize the parameters of a trial Hamiltonian and automatically find the reduced description of the original model in a way that the estimation bias and error are well controlled. The same approach can be used to construct the entanglement Hamiltonian of a quantum many-body state from its entanglement spectrum. We exemplify this using the ground states of the  $S = 1/2$  two-leg Heisenberg ladders and point out the importance of multi-spin interactions in the entanglement Hamiltonian. We observe a qualitative difference between the entanglement Hamiltonians of the two phases (the Haldane phase and the Rung Singlet phase) of the model, though their field-theoretical descriptions are almost equivalent. Possible applications to the study of strongly-correlated systems and the model construction from experimental data are discussed.

PhySH: Optimization problems, Machine learning, Strongly correlated systems, Quantum entanglement

## I. INTRODUCTION

Physical properties of classical or quantum systems are completely determined by their Hamiltonian. Therefore, the construction of the Hamiltonian for a system of interest is at the heart of physics. Traditionally, the construction has been mostly performed in an empirical manner; one would write down a simple model Hamiltonian with a few tunable parameters, and then fit them to match experimental data. These days, our knowledge of the microscopic details of the system often allows a quantitatively accurate construction of the Hamiltonian of particular materials from first principles [1–4]. However, the construction of the (effective) Hamiltonian appears also in many other contexts, and a more general and systematic method for a given microscopic model and/or experimental data is highly desired.

The construction of the Hamiltonian may be regarded as a particular case of *modeling* in the data science. This viewpoint opens up many new possibilities [5–9] to understand and exploit various data of physical systems. In particular, one can use modern tools of the data science like the machine learning (ML). Specifically speaking, we could develop a ML algorithm which automatically determines the optimized model for the given data. Such a ML approach has many advantages. For one thing, it would suffer less from the bias of each researcher or the bias can be easily controlled, because the so-called cost function gives a standard for quantifying the degree of the success of the modeling. For another, the ML can treat problems which are difficult for human beings due

to, for example, the large number of parameters or the absence of mathematically tractable methods. Although applications of the ML to physics and materials science have been actively explored [10–22] recently, these existing studies are mainly aimed to find new functional materials or to solve many-body problems (detection of the phase transitions for example), and the application for the construction of Hamiltonians is almost unexplored.

In this paper, we propose a systematic construction, or modeling, of the Hamiltonian, given its low-lying (energy or entanglement) spectrum using the ML. This is interesting in several respects. First, this gives a systematic method to construct a low-energy effective Hamiltonian with a reduced number of degrees of freedom. Second, it can deepen our understanding of quantum many-body systems through the explicit construction of their Entanglement (Modular) Hamiltonian (EH) using its spectrum, namely the Entanglement Spectrum (ES) [23]. Our algorithm would be also useful in other problems (even outside physics) where “Hamiltonian” is to be determined from its spectrum.

We show that combining the gradient descent method of the ML and the basic perturbation theory of quantum mechanics, we can update the parameters of a trial Hamiltonian securely, which eventually leads to a (local) minimum of the cost function. As a benchmark of the proposed scheme, we first apply it to the construction of the effective spin Hamiltonians of the Hubbard models at the half-filling. That is, we use the low-energy spectrum of the Hubbard model as the “experimental” data, and construct the effective spin Hamiltonian. For the homogeneous Hubbard model, we reproduce the result from the fourth order perturbation theory [24–26] under the ansatz up to the second neighbor Heisenberg interaction. We also show that even when the original Hubbard model

\* Corresponding author; h-fujita@issp.u-tokyo.ac.jp

is not translationally invariant, i.e. spatially modulated, we can optimize the local Hamiltonian at each site independently to find the effective model. In other words, using ML we can readout the symmetry breaking only from the low-energy spectrum of the original model.

We also demonstrate the construction of the EH from the ES of a given quantum many-body state. As many studies suggest, there is a similarity between the ES and the physical energy spectrum of the subsystem [23, 27–31]. Using the two-leg Heisenberg ladder [32–35] as the example, we show that the ML gives an estimate for the explicit lattice EH through the optimization of the spectrum. Away from the strongly antiferromagnetic rung limit, the EH is in general non-local as is argued in the earlier detailed analysis [35] using the full-diagonalization of the reduced density matrix. Using the ML, we find that there are fairly large contributions from the four-spin interactions in addition to those from the long-range Heisenberg interactions. Compared to the full-diagonalization approach, the ML method is based only on the low-lying spectrum, so that its computational cost is much cheaper and potentially we can access very large system sizes. We observe qualitative difference between the EH in the ferromagnetic rung phase and the antiferromagnetic rung phase, which goes beyond the field-theoretical understandings [34].

The rest of this paper is organized as follows. In Sec. II, we give a brief review of the gradient descent method and propose its implementation for the construction of Hamiltonians. In Sec. III, as a benchmark of the algorithm presented in Sec. II, we derive the effective spin model of the Hubbard models. In Sec. IV, as a more nontrivial application, we construct the EH of the two-leg Heisenberg ladder using the ES of its ground state. The final section is devoted to the conclusion and outlook, where we discuss possible applications of the presented method.

## II. GRADIENT DESCENT METHOD FOR ENERGY SPECTRUM

Here, we quickly review the basic ML algorithm, the gradient descent method, which treats the following problem: given data  $\{y_i\}$  ( $i = 1, \dots, N$ ) of our interest and the explanatory variables  $\{c_j\}$  ( $j = 1, \dots, M$ ), we identify the relation between them. Specifically speaking, we set a hypothesis like  $\tilde{y}_i = f_i(c_j)$  as a function of the parameters  $\{c_j\}$  and define a cost function  $\text{Cost}(\{c_j\}) = \frac{1}{2N} \sum_{i=1}^N (y_i - \tilde{y}_i)^2$ . This cost function measures how well the hypothesis explains the data  $\{y_i\}$  for the given parameters  $\{c_j\}$ . In the gradient descent method, we update the parameters by using the gradient of the cost function as  $c_j \rightarrow c_j - \alpha \frac{\partial \text{Cost}(\{c_j\})}{\partial c_j}$ , where  $\alpha$  is a hyperparameter called the learning rate, which is chosen by hand. If  $\alpha$  is too large, there is no guarantee that the cost decreases at each step, while if it is too small the optimization proceeds quite slowly. As long as the learning rate  $\alpha$  is properly chosen (at least not too large), the

parameter update eventually leads to a (local) minimum of the cost function.

In this paper, we construct a (spin) Hamiltonian which reproduces the given spectrum  $\{y_i\}$  ( $i = 1, \dots, N$ ) as the  $N$  lowest energy eigenvalues  $\{\tilde{y}_i\}$ . The hypothesis  $\tilde{y}_i$  is a function of coupling constants  $\{c_j\}$  ( $j = 1, \dots, M$ ) in the trial Hamiltonian  $H = \sum_{j=1}^M c_j H_j$ , where  $H_j$  can be exchange interactions, coupling with external fields, and other multi-spin interactions.

As we showed above, to apply the gradient descent method, it is essential to know the gradient of the cost function in terms of those parameters. However, the relation between the energy spectrum and the coupling constants in the Hamiltonian are quite complicated in general. Especially in correlated systems, the full parameter dependence of the cost function is in most cases unknown. Nevertheless, if the learning rate  $\alpha$  is small, the gradient itself can be analytically calculated, by using the first order perturbation theory of quantum mechanics: for given energy eigenstates of the (spin) Hamiltonian  $|\Psi_i(\{c_j\})\rangle$  and their eigenenergies  $E_i(\{c_j\})$ , we can update the parameter  $c_j$  as

$$\begin{aligned} c_j &\rightarrow c_j - \alpha \frac{\partial \text{Cost}(\{c_j\})}{\partial c_j} \\ &= c_j - \alpha \sum_{i=1}^N \frac{\partial \text{Cost}(\{c_j\})}{\partial E_i(\{c_j\})} \frac{\partial E_i(\{c_j\})}{\partial c_j} \\ &\simeq c_j - \alpha \sum_{i=1}^N \frac{\partial \text{Cost}(\{c_j\})}{\partial E_i(\{c_j\})} \langle \Psi_i | H_j | \Psi_i \rangle. \end{aligned} \quad (1)$$

In particular, if we use the mean squared error divided by two as the cost function

$$\text{Cost}(\{c_j\}) = \frac{1}{2N} \sum_{i=1}^N [y_i - E_i(\{c_j\})]^2, \quad (2)$$

we have the following update scheme for the parameters:

$$c_j \rightarrow c_j + \alpha \frac{1}{N} \sum_{i=1}^N [y_i - E_i(\{c_j\})] \langle \Psi_i | H_j | \Psi_i \rangle. \quad (3)$$

This is the central part of our strategy to construct the Hamiltonians. As long as the learning rate  $\alpha$  is small, Eq. (3) ensures that the cost improves at each step, so we can find an optimized spin Hamiltonian whose spectra achieves a (local) minimum of the cost function.

Since there is an infinite number of different Hamiltonians with exactly the same eigenvalues, the posed problem, the construction of the Hamiltonian from a given spectrum, is undetermined by nature (for  $D$  by  $D$  hermitian matrix, the number of parameters is  $D^2$ , while the number of eigenvalues we can use is at most  $D$ ). However, what we are dealing with is not a featureless Hermitian matrix, but an (entanglement) Hamiltonian of some physical systems. Therefore, we can physically set an ansatz for the spin Hamiltonian, which, for example,

possesses some symmetries or the locality of interactions. Such assumptions allow us to reduce the number of the parameters to be optimized and narrow down the candidate of the physically plausible Hamiltonian within that ansatz.

### III. BENCHMARK: LOW-ENERGY HAMILTONIAN OF HUBBARD MODEL

In the previous section, we presented a ML scheme to construct Hamiltonians from given spectra. In this section we present a benchmark of our method. We derive the effective spin models of the Hubbard models and compare them with the results from the perturbation theory.

We consider the following fermionic Hubbard chain of length  $L$  (periodic) with the spatially modulated repulsive interaction:

$$H = \sum_{i=1, \dots, L} \sum_{\sigma=\uparrow, \downarrow} t(c_{i+1, \sigma}^\dagger c_{i, \sigma} + c_{i, \sigma}^\dagger c_{i+1, \sigma}) + U_i n_i^\uparrow n_i^\downarrow \quad (4)$$

where  $U_i > 0$  is the site-dependent on-site repulsive interaction, and  $n_i^\sigma = c_{i, \sigma}^\dagger c_{i, \sigma}$  ( $\sigma = \uparrow, \downarrow$ ) is the electron density at site  $i$  with spin  $\sigma$ . Hereafter we focus on the half-filled case, so that the total number of electrons is  $L$ . We use the mean squared error Eq. (2) as the cost function in the following and take  $t = 1$ .

#### A. Homogeneous Hubbard model: comparison with the perturbation theory

First, we consider the homogeneous case with  $U_i = U$  for all  $i$  and check the consistency of the ML estimation with the perturbation theory. When the Coulomb interaction is dominantly strong  $U/t \gg 1$ , by using the second order perturbation theory in terms of  $t/U$ , we can show that the low-energy physics of the model Eq. (4) is described by the antiferromagnetic Heisenberg model. In the fourth order of  $t/U$ , in addition to the nearest-neighbor Heisenberg interaction, there appears the second neighbor Heisenberg interaction [24–26] in the effective spin model. Let us take the trial spin Hamiltonian in the form [36]

$$H = E_s + \sum_{i=1}^N \sum_{\Delta=1,2} J_\Delta \mathbf{S}_{i+\Delta} \cdot \mathbf{S}_i \quad (5)$$

where  $E_s$  is the offset and  $J_\Delta$  is the  $\Delta$ -th neighbor Heisenberg exchange coupling. We note that the fourth order perturbation theory tells that the first and the second neighbor couplings are

$$\frac{J_1^p}{t} = \frac{4t}{U} - \frac{16t^3}{U^3} + O\left(\frac{t^5}{U^5}\right) \quad (6)$$

$$\frac{J_2^p}{t} = \frac{4t^3}{U^3} + O\left(\frac{t^5}{U^5}\right), \quad (7)$$

and other terms not incorporated in Eq. (5) are  $o(t^4/U^4)$ . In the following, as the simplest benchmark, we numerically estimate the couplings ( $J_1, J_2$ ) through the optimization of the low-energy spectrum using Eq. (3) and compare them with ( $J_1^p, J_2^p$ ). We use the  $N = 50$  smallest eigenvalues of the Hubbard chain of length  $L = 10$  in the  $S^z = \sum_{i=1}^L S_i^z = 1$  sector and update the parameters with the learning rate  $\alpha = 0.1$ , until the cost stops decreasing.

In Fig. 1, we directly compare the low-lying spectra of the Hubbard model and the estimated spin model for several values of  $U$ . It shows that the estimated Hamiltonian under the ansatz Eq. (5) well reproduces the spectrum of the Hubbard model for large  $U$ . At relatively small  $U$ , we see slight deviations originating from the terms not incorporated in the present ansatz Eq. (5). We also notice that at large  $U$ , where the fourth order term is also inessential, the normalized spectrum becomes independent of  $U/t$ , since the spectrum is converged to that of the Heisenberg model with  $J_1 = 1$ .

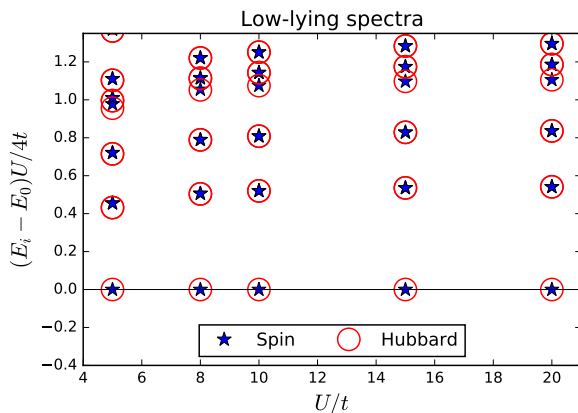


FIG. 1. Direct comparison of the spectrum (in the  $S_z = 1$  sector) of the Hubbard model (red circles) and of the estimated spin model (blue stars) under the ansatz Eq. (5). For large  $U/t$  the estimated spin Hamiltonian reproduces the low-lying spectrum of the Hubbard model.

To compare the estimated Hamiltonian with that of the perturbation theory, we show the  $U$  dependence of the difference  $|J_\Delta - J_\Delta^p|$  and the cost under the ansatz Eq. (5) in Fig. 2. We see that at large  $U$ , the difference decays as  $U^{-5}$  and the cost Eq. (2) as  $U^{-10}$ , which are consistent with the perturbation theory. The  $U^{-10}$  dependence of the cost indicates that the ansatz Eq. (5) contains all the terms appearing in the fourth order perturbation theory [which is valid at  $O(t^4/U^4)$ ], and the optimization achieves the global minimum (at least quite close to that) of the cost function within the present ansatz.

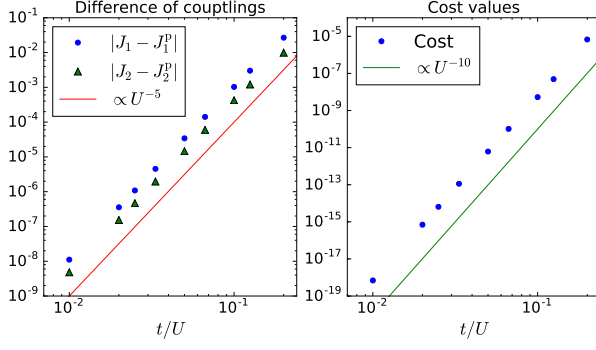


FIG. 2. Left panel: Comparison of exchange couplings obtained by the perturbation theory  $J_{\Delta}^p$  and by the optimization scheme Eq. (3). Their difference depends on  $U$  as  $U^{-5}$  for large  $U$ , indicating that the proposed scheme Eq. (3) can reproduce the perturbative results. Right panel:  $U$  dependence of the cost function Eq. (2). The cost, mean squared error of the estimation, depends on  $U$  as  $\propto U^{-10}$ . We use the lowest  $N = 50$  eigenvalues for the optimization with the learning rate  $\alpha = 0.1$ .

### B. Periodically modulated Hubbard model

Concerning the homogeneous Hubbard chain, we show that the ML scheme works well and reproduces the known perturbative results. Next we turn on the inhomogeneity in Eq. (4), which breaks the translational symmetry. For simplicity, we take a large repulsive interaction where only the nearest-neighbor spin interaction would matter and we can use the perturbative results as a reference. We take the trial spin Hamiltonian in the form:

$$H = E_s + \sum_{i=1}^L J_{1,i} \mathbf{S}_i \cdot \mathbf{S}_{i+1}. \quad (8)$$

The exchange couplings are optimized in a site-dependent way, so that the number of parameters scales with the system volume (precisely given by  $L + 1$  including  $E_s$ ). We take the following initial values inferred from the second order perturbation theory of the homogeneous Hubbard model:  $J_{1,i} = 4(1 + 0.01\xi_i)t^2/U_i$ , where  $\xi_i$  is a random number taken from the standard normal distribution  $\mathcal{N}(0,1)$ . The randomness is introduced to resolve the ambiguity of the phase of the spatial modulation in the spin model (we only use the energy spectrum of a periodic Hubbard chain). The initial value for the offset  $E_s$  is taken to be at the middle of the energy window  $[E_1, E_N]$ ,  $E_s = (E_1 + E_N)/2$ .

We consider the Hubbard chain of length  $L = 13$  with the repulsive interaction  $U_n = U[1 - 0.1\sin(2\pi n/L)]$ , where  $U/t = 50$ . We take the learning rate  $\alpha = 0.3$  and update the parameters  $J_i$  using the proposed update scheme Eq. (3) for the lowest  $N = 30$  eigenvalues in the  $S^z = \sum_{i=1}^L S_i^z = 4.5$  sector. In Fig. 3, we present the spatial profile of the estimated exchange couplings  $J_i$  for  $i = 1, \dots, L$ . We see that as the learning

proceeds, the estimated exchange couplings approach to  $J_{1,i} = 4t^2/U_i$  [37], which we naively expect from the perturbation theory of the homogeneous Hubbard model. It demonstrates that our scheme works even in the absence of the translational symmetry and can extract the information of the symmetry breaking only from the low-lying spectrum. It also implies that our method works for more generic boundary conditions other than the periodic boundary condition.

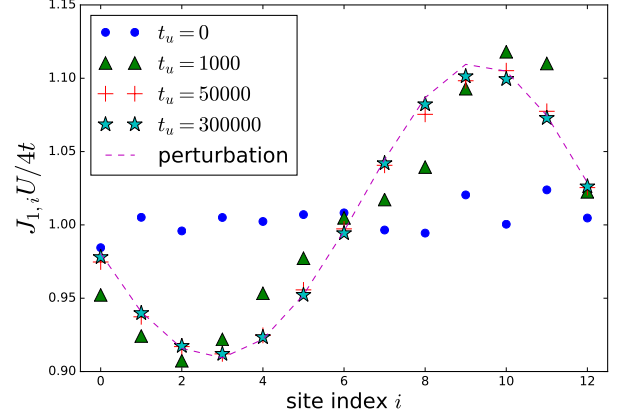


FIG. 3. Spatial profile of the nearest-neighbor exchange couplings estimated from the lowest  $N = 30$  eigenvalues ( $S_z = 4.5$  sector) of the Hubbard model Eq. (4) with  $U_n = 50[1 - 0.1\sin(2\pi n/L)]$  ( $n = 1, \dots, L = 13$ ). We use  $\alpha = 0.3$  and update the parameters  $t_u = 300,000$  times and compare the estimated parameters (markers) with those expected from the second order perturbation theory (broken line). The optimized parameters reproduce the spatial modulation of the original Hubbard Hamiltonian.

### IV. CONSTRUCTION OF ENTANGLEMENT HAMILTONIAN

As a more nontrivial application of our scheme, here we show that our approach works for the construction of the EH from the ES of a given quantum many-body state.

First we briefly review the definition of the ES and the EH. Let us consider spin systems consisting of two subregions  $A$  and  $B$ . For a given quantum state  $|\Psi\rangle$  defined on  $A \cup B$ , we introduce the reduced density matrix of the subregion  $A$  by tracing out the spin degrees of freedom in the region  $B$ :

$$\rho_A = \text{Tr}_B |\Psi\rangle \langle \Psi|. \quad (9)$$

The EH is defined as the Hamiltonian whose density matrix at the unit temperature is the reduced density matrix:  $\rho_A \equiv e^{-H_A}$ . The ES is defined as its eigenvalues [23], which reflects the non-local quantum correlation between the subregions  $A$  and  $B$ .

The ES and EH are defined through the entanglement cut, the *virtual* separation of the given quantum state into two parts. Nevertheless, there is an intriguing conjecture that they are related to physical edge spectrum and Hamiltonian which appear when the system is actually (not virtually) cut into two parts [23, 29]. This conjecture is confirmed in, for example, the two-dimensional topological phase, where there appear chiral edge modes described by the conformal field theory at the physical boundary. In lattice systems, the canonical example of this correspondence is found in the Affleck-Kennedy-Lieb-Tasaki (AKLT) chain [38–42], a variant of the  $S = 1$  antiferromagnetic Heisenberg chain. The ground state of the AKLT chain is written in terms of singlet bonds between the emergent  $S = 1/2$  degrees of freedom, and on both the virtual and the physical edges, there appears the free  $S = 1/2$  degrees of freedom.

As we mentioned in the introductory part, EH cannot be uniquely determined from a given ES, even in principle. However, as implied by the entanglement/edge correspondence conjecture [23, 29], we may expect EH to be “local”, as long as the original model is so. With the requirement of the locality, EH can be practically estimated by the ES, as we will demonstrate below.

As a concrete example, let us discuss the two-leg periodic  $S = 1/2$  antiferromagnetic Heisenberg ladder with  $A$  and  $B$  legs

$$H = \sum_{i=1}^L J_{\text{rung}} \mathbf{S}_{i,A} \cdot \mathbf{S}_{i,B} + \sum_{i=1}^L \sum_{j=A,B} J_{\text{leg}} \mathbf{S}_{i,j} \cdot \mathbf{S}_{i+1,j}. \quad (10)$$

We introduce two kinds of interactions,  $J_{\text{leg}}$  and  $J_{\text{rung}}$ . The former describes the intra-chain interaction and the latter does the inter-chain one. The ground state phase diagram of Eq. (10) for  $J_{\text{leg}} = J \cos \theta$ ,  $J_{\text{rung}} = J \sin \theta$  is given in Fig. 4 (a) [32, 43, 44].

Following Refs. [32–35, 45], here we study the entanglement for a virtual cut which separates the chains as shown in Fig. 4 (b). The EH then acts on the Hilbert space of a single  $S = 1/2$  chain. In Ref. [32], it was argued that the EH is qualitatively given by the  $S = 1/2$  Heisenberg chain based on the numerically obtained ES. However, since the identification was made by a visual inspection of the spectrum, it is difficult to analyze its accuracy and possible corrections to the simple Heisenberg model quantitatively. If we have access to all the eigenvectors of the reduced density matrix, as is performed in Ref. 35 we can construct the EH exactly within a particular ansatz. However, the full-diagonalization of large matrices is computationally heavy and its applicability is limited to small subsystems. In the following, we show that our ML scheme offers another approach for the construction of the EH. In the final part of this section, we compare the ML approach with the full-diagonalization approach in detail.

Below we focus on the ground state of the model Eq. (10) and estimate the EH using the  $N$  smallest ES, not the entire eigenvectors of the reduced density matrix. As the trial Hamiltonian for  $H_A$ , we use the following  $SU(2)$  symmetric spin Hamiltonian,

$$H = E_s + \sum_{i=1}^L \sum_{\delta=1,2,3} J_{\delta} \mathbf{S}_i \cdot \mathbf{S}_{i+\delta} + \sum_{i=1}^L \sum_{\alpha,\beta,\gamma=\{1,2,3\}} \frac{K_{\alpha}}{2} (\mathbf{S}_i \cdot \mathbf{S}_{i+\alpha})(\mathbf{S}_{i+\beta} \cdot \mathbf{S}_{i+\gamma}) \quad (11)$$

where  $E_s$ ,  $J_{\delta}$ , and  $K_{\alpha}$  are the parameters to be determined through the optimization of the spectrum. Here the summation over  $\alpha, \beta, \gamma = 1, 2, 3$  is taken under the condition  $\alpha \neq \beta \neq \gamma$  and  $\alpha \neq \gamma$ . We take into account the long-range Heisenberg interactions up to the third neighbor and the three simplest four-spin interactions. In the previous work [35] based on the full-diagonalization of the reduced density matrix, the coupling constants of the two-body interactions up to the seventh neighbors were estimated, but other multi-spin interactions were treated all together and their individual contributions were not obtained. Here we incorporate the four-spin interactions and reveal their importance quantitatively using the ML.

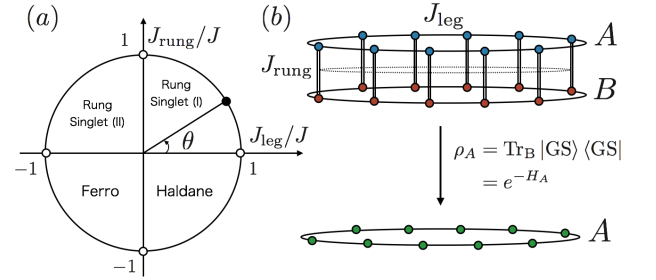


FIG. 4. (a) Ground state phase diagram of the model Eq. (11). (b) Schematic diagram of the definition of the entanglement Hamiltonian for the leg-separating cut. The dotted line indicates the entanglement cut.

When the rung interaction is dominantly strong and antiferromagnetic ( $\theta \simeq \pi/2$ ), for each  $i$ , the spins in the two legs  $\mathbf{S}_{i,A}$  and  $\mathbf{S}_{i,B}$  form a singlet, so the virtual cut produces  $S = 1/2$  spins at each singlet bond as we mentioned in relation to the AKLT model. In the presence of the strong rung repulsion, therefore, we have well-defined  $S = 1/2$  degrees of freedom at each site in the EH. Away from  $\theta = \pi/2$ , tracing out the leg  $B$  makes the EH of the leg  $A$  non-local. In particular, the situation is quite nontrivial when the rung interaction is weakly antiferromagnetic or ferromagnetic. In these cases, long-range and multi-spin interactions would be important to reproduce the ES. In other words, the ansatz Eq. (11) becomes no longer the proper one and the cost will increase.

The estimation of the EH proceeds as follows. We first obtain the ground state wave function of the model Eq. (10) in the  $S_{\text{tot}}^z = \sum_i S_i^z = 0$  sector and calculate

the reduced density matrix  $\rho_A$  by tracing out the chain  $B$ . The ES are obtained by diagonalizing  $\rho_A$  and we optimize the trial spin Hamiltonian Eq. (11) using the algorithm Eq. (3). We consider the ladder with length  $L = 10$ , and take the  $N = 100$  smallest eigenvalues in the  $S_A^z = \sum_{i \in A} S_i^z = 1$  sector for the optimization [46]. As we mention later, the choice of the symmetry sector (the value of  $S_A^z$ ) is arbitrary in our method. We update parameters under  $\alpha = 0.3$  until the value of the cost function Eq. (2) stops decreasing.

Since the estimated parameters generically correspond to a local, not necessarily the global, minimum of the cost function, we employ random initialization of the parameters. By using the ES  $\{E_i\}_{i=1,\dots,N}$ , we set the initial values of the parameters as  $E_s = (E_1 + E_N)/2$ ,  $J_1 = \text{sign}(J_{\text{leg}})(E_N - E_1)/2$ , and  $J_{\delta>1}, K_{\alpha=1,2,3} \in 0.1 \times \mathcal{N}(0, 1)$ . Namely, we take the offset  $E_s$  as the center of the energy window  $[E_1, E_N]$  and take the nearest-neighbor exchange  $J_1$  as a half the width of  $[E_1, E_N]$ , and initialize other parameters randomly by using the standard normal distribution  $\mathcal{N}(0, 1)$ . For different initial values chosen in this way, we perform the optimization for each  $\theta$ . Physically, here we expect that the nearest-neighbor coupling is large in magnitude as compared to the other couplings, and that the sign of the nearest-neighbor coupling is the same as of the original two-leg ladder model Eq. (10).

In Fig. 5 we show the  $\theta$  dependence of the estimated parameters and the cost function Eq. (2) for the run reached to the lowest value of the cost function among 100 trials for each  $\theta$ . Although our ansatz for the EH is different from the one used in Ref. 35, we obtain consistent results as discussed below. To quantify the possible error in our estimation of the coupling constants, we use the square root of the cost function  $2\text{Cost}(\theta)/J_1^2$  as an estimate for the error bars of the estimated parameters in the figure (only to  $K_3/J_1$  for visibility). The deviation between the ES and the spectrum of the spin model Eq. (11) is caused either by the deadlock in a non-global minimum of the cost function or by the failure of this ansatz.

When both the rung and the leg interactions are ferromagnetic ( $-\pi < \theta < -\pi/2$ ) the ground state is ferromagnetically ordered, and there is no entanglement between the two chains. In the following, we discuss the results in the other regions of the phase diagram Fig. 4(a).

### 1. Antiferromagnetic rung region, $0 < \theta < \pi$

When  $\theta = \pi/2$ , the system turns into a decoupled  $L$  singlets and the ES is completely degenerate, so that the EH is zero and can be considered as the Hamiltonian of the (locally) independent  $S = 1/2$  spins. In Fig. 5, we see that even away from this trivial limit, the short-ranged ansatz Eq. (11) well reproduces the ES when the rung is antiferromagnetic. In the limit  $\theta \rightarrow \pi/2$ , we find that the EH is dominated by the nearest-neighbor Heisenberg interaction  $J_1$  (all the other couplings in Eq. (11) van-

ish relative to  $J_1$ ) so that the correspondence with the nearest-neighbor Heisenberg chain becomes almost exact. We note the estimated  $J_1$  has the same sign as  $J_{\text{rung}}$ , as we expected in choosing the initial values of the learning. These observations are consistent with Refs. 32 and 35.

However, the value of the cost function rapidly grows as  $\theta$  approaches to  $\theta = 0, \pi$ , and at the same time, coupling constants of further neighbor and multi-spin interactions become large. The largest correction comes from the second neighbor Heisenberg interaction in consistent with the previous study [33] using the perturbation theory near the strong rung limit and the full-diagonalization approach [35]. In addition to the long-range Heisenberg interactions, we observe fairly large contributions from the four-spin interaction terms, which are not explicitly known in these previous works. We see that near  $\theta = 0$  the coupling constants of these terms become comparable and even larger than the second neighbor Heisenberg interaction. The large estimation error and the growth of coupling constants imply that, far away from  $\theta \simeq \pi/2$ , the short-ranged Hamiltonian Eq. (11) is no longer a valid ansatz. To reproduce the ES in this case, therefore, we have to refine the ansatz and include further neighbor couplings and other kinds of multi-spin interactions.

### 2. Ferromagnetic rung region, $-\pi/2 < \theta < \pi$

In this region, called the Haldane phase, there is a small but finite inter-leg entanglement in the ground state as opposed to the ferromagnetic phase. In the earlier studies [32, 33, 35], it was argued that the EH in this phase is also qualitatively given by the antiferromagnetic Heisenberg chain, similarly to the Rung Singlet (I) phase.

We see that estimation error under the short-ranged, two-body Hamiltonian ansatz Eq. (11) is large for all  $\theta$  in this region  $-\pi/2 < \theta < 0$ . Moreover, the estimated coupling constants show apparently non-systematic  $\theta$  dependence, indicating the instability of the estimation due to the failure of the ansatz. In particular, near  $\theta = 0$ , the estimated coupling constant  $K_1$  (one of the four-spin interactions) becomes very large and exceeds the nearest neighbor Heisenberg coupling.

Although the estimation error in this region is large and the interpretation of the estimated parameters is nontrivial, our result implies that the actual EH in the Haldane phase would be not at all a simple Heisenberg-like model as opposed to the  $\theta \simeq \pi/2$  region. Such a large contribution from the four-spin interaction is not explicitly discussed in the previous study [35]. As we mentioned, in Ref. 35 the contributions from the multi-spin interactions are treated all together. Therefore, their estimation for the multi-spin couplings is a lower-bound, and each multi-spin term could be very large in principle as is observed above.

We note that, the ES in the Rung Singlet (I) and Haldane phases can be discussed in the field theory



(bosonization) approach [34]. In this picture, these two phases correspond to the case in which two boson fields (symmetric and antisymmetric between two legs) are both gapped. The difference between the two phases is given by the different location of the potential minimum to which the boson field is pinned. However, this difference essentially does not affect the ES, and the ES is shown to be given by the energy spectrum of a Tomonaga-Luttinger Liquid. In fact, many different microscopic Hamiltonians, including those with some degree of long-range interactions [47, 48] are described by the same effective field theory (Tomonaga-Luttinger Liquid) in the low-energy limit. The apparent long-range interactions in the EH we obtain (and also found in Ref. 35), for the Haldane phase do not immediately contradict with the field-theoretical result [34], but it implies that there are still many uncovered issues related to the entanglement/edge correspondence beyond the low-energy, or field-theoretical region.

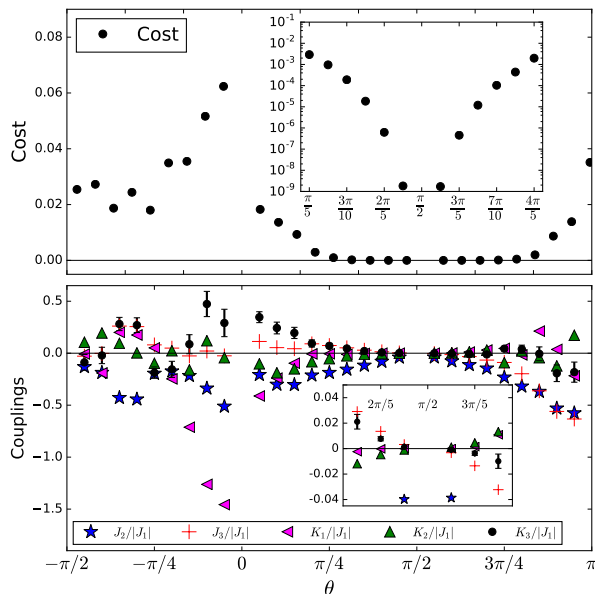


FIG. 5. Cost function and the corresponding coupling constants  $J_\delta/J_1$  ( $\delta = 2, 3$ ),  $K_\alpha/J_1$  ( $\alpha = 1, 2, 3$ ) as functions of  $\theta$ . The shown cost and couplings are of the best run among 100 trials from randomly selected initial parameters for each  $\theta$  with  $\alpha = 0.3$  and  $N = 100$ . Near  $\theta = \pi/2$ , the estimated entanglement Hamiltonian Eq. (11) contains almost only the nearest-neighbor Heisenberg interaction. As  $\theta$  deviates from this special point, long-range and many-body interactions become important and the ansatz Eq. (11) breaks down, resulting in the apparent growth of the cost. In the insets, we show the cost and coupling constants near the rung singlet limit  $\theta = \pi/2$ . The error bars indicate twice the square root of the cost function.

In the above, we consider the simplest entanglement cut, which preserves the translational symmetry in the leg direction. However, as we mentioned in the previous section, the ML scheme could be applied to systems with generic boundary conditions. In the context of EH, it

means that we can construct the EH for the arbitrary entanglement cuts, which generically break the translational invariance of the subsystem.

Finally, we compare our ML approach for the construction of the EH with the full-diagonalization approach [35] in more detail. When the subsystem size is small and all the eigenvectors of the reduced density matrix are available, the full-diagonalization approach gives a more reliable estimate for the EH, since it is, in principle, exact. However, as we mentioned, the difficulty comes into play when one tries to estimate the EH of large subsystems. In particular, when the translational symmetry is absent, which is the generic situation due to the entanglement cuts, the possible subsystem size is at present up to about 21-22 sites of  $S = 1/2$  spins even if we assume the conservation of the total magnetization. By contrast, our ML scheme only uses the low-lying spectrum of the reduced density matrix, so that one can exploit the computationally cheap algorithms for the matrix diagonalization such as the Lanczos method and construct the EH for much larger subsystems. Hence, the full-diagonalization approach [35] and our ML approach will work complementary for the reliable estimation of the EH; the former is particularly suitable for small subsystems and can determine the reasonable form of the ansatz of the EH, while the latter can optimize that ansatz for much larger subsystems.

It is also worth mentioning that in the presence of the symmetries like the conservation of the total magnetization, choosing the proper symmetry sector of that symmetry further increases the possible subsystem size in the ML approach. Our approach can be applied to the low-lying spectrum of a particular symmetry sector, so that we can avoid the sector with the large Hilbert space dimension. For example, when the total magnetization of the subsystem is conserved, one can use the spectrum in the high spin sector (large  $S_A^z$  sector) of the reduced density matrix, whose Hilbert space dimension is orders of magnitude smaller than that of the computationally heaviest sector with  $S_A^z = 0$ . This could change the bottleneck of the construction of the EH from the diagonalization of the reduced density matrix to the derivation of the (ground state) wave function. The wave function of the ground state (and also the low-lying states) of many-body systems is sometimes available for quite large system sizes by using the tailor-made algorithms such as the Density Matrix Renormalization Group (DMRG) [49, 50]. Therefore, combined with the DMRG and the full-diagonalization for small subsystems, our ML approach could give the reliable estimate for the EH in the extremely large subsystems.

## V. CONCLUSION AND OUTLOOK

In this paper, we developed a machine learning algorithm to construct (spin) Hamiltonians from the energy or entanglement spectra. As a benchmark, we first con-

sider the Hubbard models and use the proposed scheme to estimate the effective spin Hamiltonians. For the homogeneous Hubbard model, we show that the machine learning can reproduce the result from the fourth order perturbation theory [24–26] just through the optimization of the energy spectrum. We also demonstrate that from the energy spectrum we can infer the breaking of the translational symmetry in the periodically modulated Hubbard model. Moreover, we show that the same algorithm can be applied to construct the entanglement Hamiltonian from the entanglement spectrum of a given quantum many-body state, taking the two-leg antiferromagnetic Heisenberg ladder as the example. We observe a qualitative difference between the Rung Singlet (I) and Haldane phases, which goes beyond the field-theoretical description, in consistent with the earlier study [35] based on the full-diagonalization of the reduced density matrix. We point out the importance of the four-body interactions, which is not explicitly known in the previous works. Since the machine learning approach only uses the low-lying entanglement spectrum and does not require the full-diagonalization of the reduced density matrix, it can be applied to larger subsystem sizes. If combined with the Density Matrix Renormalization Group, it offers a way to examine the celebrated entanglement/edge correspondence for the unprecedentedly large system sizes.

Here, we comment on the possible application of the presented scheme to experimental data, rather than the numerically obtained the numerically obtained energy spectrum. In this paper, as the simplest example, we use the mean squared error of the energy spectrum as the cost function and optimize the Hamiltonian. However, the choice of the cost function or the quantity to be optimized is not restricted to that. The heart of the presented strategy is the fact that the gradient of the energy spectrum can be analytically obtained using the knowledge of the perturbation theory in quantum mechanics. Therefore, as long as the cost is defined as a function of the energy spectrum, essentially the same procedure gives the optimized Hamiltonian. For example, we could use the experimentally obtained density of states (and thus specific heat) and the corresponding numerical data of the trial Hamiltonian to define the cost function for the optimization.

Another important application of our method is for the study of the strongly-correlated electron systems, modeled by the Hubbard-like Hamiltonians. Although we focused on the one-dimensional systems in Sec. 3 for simplicity, our approach, optimization of the energy spectrum with the machine learning, should work for general dimensions, especially for two dimensions. The Hubbard model in two dimensions is one of the most important subjects in the modern condensed matter physics in the context of high temperature superconductivity in cuprates [51] and quantum spin liquids [52–57]. The main advantage of our approach is that it can be readily applied

to the  $t/U \sim 1$  region where various nontrivial physics takes place from the competition between the kinetic energy and the interaction energy. In this region, perturbative treatment breaks down or becomes hard to be performed. Nevertheless our scheme still works and gives an estimate of the effective spin Hamiltonian as long as there exists a charge gap and the spin-model description is possible in the low-energy sector. Even when the original Hubbard model is more complicated, e.g. contains the further neighbor hoppings, long-range interactions, or disorders, the present method can be straightforwardly applied to that.

Since the dimension of the Hilbert space is reduced from  $4^L$  to  $2^L$  through the derivation of the effective spin model, the above procedure can be regarded as a compression of the Hilbert space and doubles the achievable system size in the numerical calculations of the Hubbard-like models. Therefore, with our numerical optimization approach one can investigate the low-energy properties of the (two-dimensional) Hubbard models at the half-filling with unconventionally large system sizes. Although the size dependence of the optimized parameters obtained by our method may require careful treatments, this would offer a new approach for the various unsolved issues in the strongly-correlated electron systems, such as the ground state property of the Hubbard-like systems on the triangular lattice [52, 53, 55, 58, 59]

Lastly, we note that in this paper we employ the simplest “batch” gradient descent method to ensure the cost decreases monotonically. Since the batch gradient descent method is the root of various machine learning algorithms, our results are compatible with more sophisticated machine learning methods. For example, we can trivially extend the update scheme Eq. (3) to the stochastic gradient descent method, which would be computationally more economic, though in turn, there is no guarantee that the cost improves monotonically.

## VI. ACKNOWLEDGEMENT

We thank M. Ohzeki, S. Furukawa, and Y. Fuji for useful comments and discussions. H. F. and Y. O. N are supported by Advanced Leading Graduate Course for Photon Science (ALPS) of Japan Society for the Promotion of Science (JSPS). The works of H. F., Y. O. N., and S. S are supported by JSPS KAKENHI Grant-in-Aid for JSPS Fellows Grant No. JP16J04752, No. JP16J01135, and No. JP15J11250, respectively. The work of M. O. is supported in part by JSPS KAKENHI Grant No. 16K05469. A part of the computation in this work has been done using the facilities of the Supercomputer Center, the Institute for Solid State Physics, the University of Tokyo. H. F. thanks SPICE, JGU Mainz, where a part of this study was done.



- 
- [1] Kazuma Nakamura, Ryotaro Arita, and Masatoshi Imada, “Ab initio Derivation of Low-Energy Model for Iron-Based Superconductors LaFeAsO and LaFePO,” *Journal of the Physical Society of Japan* **77**, 093711 (2008).
- [2] Kazuma Nakamura, Yoshihide Yoshimoto, Taichi Kosugi, Ryotaro Arita, and Masatoshi Imada, “Ab initio Derivation of Low-Energy Model for -ET Type Organic Conductors,” *Journal of the Physical Society of Japan* **78**, 083710 (2009).
- [3] Takashi Miyake, Ferdi Aryasetiawan, and Masatoshi Imada, “Ab initio procedure for constructing effective models of correlated materials with entangled band structure,” *Phys. Rev. B* **80**, 155134 (2009).
- [4] Youhei Yamaji, Yusuke Nomura, Moyuru Kurita, Ryotaro Arita, and Masatoshi Imada, “First-Principles Study of the Honeycomb-Lattice Iridates  $\text{Na}_2\text{IrO}_3$  in the Presence of Strong Spin-Orbit Interaction and Electron Correlations,” *Phys. Rev. Lett.* **113**, 107201 (2014).
- [5] M. Ohzeki, “L1-Regularized Boltzmann Machine Learning Using Majorizer Minimization,” *Journal of the Physical Society of Japan* **84**, 054801 (2015).
- [6] Mareki Honma, Kazunori Akiyama, Fumie Tazaki, Kazuki Kuramochi, Shiro Ikeda, Kazuhiro Hada, and Makoto Uemura, “Imaging black holes with sparse modeling,” *Journal of Physics: Conference Series* **699**, 012006 (2016).
- [7] Junya Otsuki, Masayuki Ohzeki, Hiroshi Shinaoka, and Kazuyoshi Yoshimi, “Sparse modeling approach to analytical continuation of imaginary-time quantum Monte Carlo data,” arXiv: 1702.03056 (2017).
- [8] Koji Hukushima Masamichi J. Miyama, “Real-space analysis of scanning tunneling microscopy topography datasets using sparse modeling approach,” arXiv: 1703.0843 (2017).
- [9] Ryo Tamura and Koji Hukushima, “Method for estimating spin-spin interactions from magnetization curves,” *Phys. Rev. B* **95**, 064407 (2017).
- [10] Aaron Gilad Kusne, Tieren Gao, Apurva Mehta, Liqin Ke, Manh Cuong Nguyen, Kai-Ming Ho, Vladimir Antropov, Cai-Zhuang Wang, Matthew J. Kramer, Christian Long, and Ichiro Takeuchi, “On-the-fly machine-learning for high-throughput experiments: search for rare-earth-free permanent magnets,” *Scientific Reports* **4**, 6367 EP – (2014).
- [11] Luca M. Ghiringhelli, Jan Vybiral, Sergey V. Levchenko, Claudia Draxl, and Matthias Scheffler, “Big Data of Materials Science: Critical Role of the Descriptor,” *Phys. Rev. Lett.* **114**, 105503 (2015).
- [12] Sergei V. Kalinin, Bobby G. Sumpter, and Richard K. Archibald, “Big-deep-smart data in imaging for guiding materials design,” *Nat Mater* **14**, 973–980 (2015).
- [13] Peter Broecker, Juan Carrasquilla, Roger G. Melko, and Simon Trebst, “Machine learning quantum phases of matter beyond the fermion sign problem,” arXiv: 1608.07848 (2016).
- [14] Kelvin Ch’ng, Juan Carrasquilla, Roger G. Melko, and Ehsan Khatami, “Machine Learning Phases of Strongly Correlated Fermions,” arXiv: 1609.02552 (2016).
- [15] Tomoki Ohtsuki and Tomi Ohtsuki, “Deep Learning the Quantum Phase Transitions in Random Two-Dimensional Electron Systems,” *Journal of the Physical Society of Japan* **85**, 123706 (2016).
- [16] Yi Zhang and Eun-Ah Kim, “Quantum loop topography for machine learning,” arXiv:1611.01518 (2016).
- [17] Dong-Ling Deng, Xiaopeng Li, and S. Das Sarma, “Exact Machine Learning Topological States,” arXiv:1609.09060 (2016).
- [18] Frank Schindler, Nicolas Regnault, and Titus Neupert, “Probing many-body localization with neural networks,” arXiv: 1704.01478 (2017).
- [19] Giuseppe Carleo and Matthias Troyer, “Solving the quantum many-body problem with artificial neural networks,” *Science* **355**, 602–606 (2017).
- [20] Evert P. L. van Nieuwenburg, Ye-Hua Liu, and Sebastian D. Huber, “Learning phase transitions by confusion,” *Nat Phys* **13**, 435–439 (2017).
- [21] Juan Carrasquilla and Roger G. Melko, “Machine learning phases of matter,” *Nat Phys* **13**, 431–434 (2017).
- [22] Yi Zhang, Roger G. Melko, and Eun-Ah Kim, “Machine learning  $\mathbb{Z}_2$  quantum spin liquids with quasi-particle statistics,” arXiv: 1705.01947 (2017).
- [23] Hui Li and F. D. M. Haldane, “Entanglement Spectrum as a Generalization of Entanglement Entropy: Identification of Topological Order in Non-Abelian Fractional Quantum Hall Effect States,” *Phys. Rev. Lett.* **101**, 010504 (2008).
- [24] D. J. Klein and W. A. Seitz, “Perturbation Expansion of the Linear Hubbard Model,” *Phys. Rev. B* **8**, 2236–2247 (1973).
- [25] Minoru Takahashi, “Half-filled Hubbard model at low temperature,” *J.Phys. C* **10**, 1289 (1977).
- [26] A. H. MacDonald, S. M. Girvin, and D. Yoshioka, “ $\frac{t}{U}$  expansion for the Hubbard model,” *Phys. Rev. B* **37**, 9753–9756 (1988).
- [27] Ingo Peschel and Ming-Chiang Chung, “On the relation between entanglement and subsystem Hamiltonians,” *EPL (Europhysics Letters)* **96**, 50006 (2011).
- [28] Anushya Chandran, M. Hermanns, N. Regnault, and B. A. Bernevig, “Bulk-edge correspondence in entanglement spectra,” *Phys. Rev. B* **84**, 205136 (2011).
- [29] Xiao-Liang Qi, Hosho Katsura, and Andreas W. W. Ludwig, “General Relationship between the Entanglement Spectrum and the Edge State Spectrum of Topological Quantum States,” *Phys. Rev. Lett.* **108**, 196402 (2012).
- [30] Brian Swingle and T. Senthil, “Geometric proof of the equality between entanglement and edge spectra,” *Phys. Rev. B* **86**, 045117 (2012).
- [31] J. Dubail, N. Read, and E. H. Rezayi, “Edge-state inner products and real-space entanglement spectrum of trial quantum Hall states,” *Phys. Rev. B* **86**, 245310 (2012).
- [32] Didier Poilblanc, “Entanglement Spectra of Quantum Heisenberg Ladders,” *Phys. Rev. Lett.* **105**, 077202 (2010).
- [33] Andreas M. Läuchli and John Schliemann, “Entanglement spectra of coupled  $s = \frac{1}{2}$  spin chains in a ladder geometry,” *Phys. Rev. B* **85**, 054403 (2012).
- [34] Rex Lundgren, Yohei Fuji, Shunsuke Furukawa, and Masaki Oshikawa, “Entanglement spectra between coupled Tomonaga-Luttinger liquids: Applications to ladder systems and topological phases,” *Phys. Rev. B* **88**, 245137 (2013).

- [35] J. I. Cirac, Didier Poilblanc, Norbert Schuch, and Frank Verstraete, “Entanglement spectrum and boundary theories with projected entangled-pair states,” *Phys. Rev. B* **83**, 245134 (2011).
- [36] As we mentioned in the introduction, physically we can require symmetries and locality to set the ansatz for the trial Hamiltonian. Here for simplicity we just incorporate terms appearing in the fourth order perturbation theory.
- [37] As we mentioned, the phase of the spatial modulation of the spin model is ambiguous. In Fig. 3 we choose the phase  $\phi$  as a fitting parameter and plot  $J_{1,i} = 4t^2/U_i$  with  $U_n = U[1 - 0.1 \sin(2\pi n/L + \phi)]$  for the  $\phi$  reproducing the  $t_u = 300000$  result best.
- [38] Ian Affleck, Tom Kennedy, Elliott H. Lieb, and Hal Tasaki, “Rigorous results on valence-bond ground states in antiferromagnets,” *Phys. Rev. Lett.* **59**, 799–802 (1987).
- [39] Ian Affleck, Tom Kennedy, Elliott H. Lieb, and Hal Tasaki, “Valence bond ground states in isotropic quantum antiferromagnets,” *Communications in Mathematical Physics* **115**, 477–528 (1988).
- [40] Frank Pollmann, Ari M. Turner, Erez Berg, and Masaki Oshikawa, “Entanglement spectrum of a topological phase in one dimension,” *Phys. Rev. B* **81**, 064439 (2010).
- [41] Ari M. Turner, Frank Pollmann, and Erez Berg, “Topological phases of one-dimensional fermions: An entanglement point of view,” *Phys. Rev. B* **83**, 075102 (2011).
- [42] Frank Pollmann, Erez Berg, Ari M. Turner, and Masaki Oshikawa, “Symmetry protection of topological phases in one-dimensional quantum spin systems,” *Phys. Rev. B* **85**, 075125 (2012).
- [43] T. Barnes, E. Dagotto, J. Riera, and E. S. Swanson, “Excitation spectrum of Heisenberg spin ladders,” *Physical Review B* **47**, 3196–3203 (1993).
- [44] Elbio Dagotto and T. M. Rice, “Surprises on the Way from One- to Two-Dimensional Quantum Magnets: The Ladder Materials,” *Science* **271**, 618 (1996).
- [45] Shunsuke Furukawa and Yong Baek Kim, “Entanglement entropy between two coupled Tomonaga-Luttinger liquids,” *Phys. Rev. B* **83**, 085112 (2011).
- [46] The entanglement cut considered here preserves the  $z$  component of the total spin, so that the EH can be block-diagonalized in terms of  $S_A^z$ .
- [47] F. D. M. Haldane, “Exact Jastrow-Gutzwiller resonating-valence-bond ground state of the spin-(1/2 antiferromagnetic Heisenberg chain with  $1/r^2$  exchange,” *Phys. Rev. Lett.* **60**, 635–638 (1988).
- [48] B. S. Shastry, “Exact solution of an  $S=1/2$  Heisenberg antiferromagnetic chain with long-ranged interactions,” *Phys. Rev. Lett.* **60**, 639–642 (1988).
- [49] Steven R. White, “Density matrix formulation for quantum renormalization groups,” *Phys. Rev. Lett.* **69**, 2863–2866 (1992).
- [50] U. Schollwöck, “The density-matrix renormalization group,” *Rev. Mod. Phys.* **77**, 259–315 (2005).
- [51] Elbio Dagotto, “Correlated electrons in high-temperature superconductors,” *Rev. Mod. Phys.* **66**, 763–840 (1994).
- [52] Y. Shimizu, K. Miyagawa, K. Kanoda, M. Maesato, and G. Saito, “Spin Liquid State in an Organic Mott Insulator with a Triangular Lattice,” *Phys. Rev. Lett.* **91**, 107001 (2003).
- [53] Peyman Sahebsara and David Sénéchal, “Hubbard Model on the Triangular Lattice: Spiral Order and Spin Liquid,” *Phys. Rev. Lett.* **100**, 136402 (2008).
- [54] J.-Y. P. Delannoy, M. J. P. Gingras, P. C. W. Holdsworth, and A.-M. S. Tremblay, “Low-energy theory of the  $t - t' - t'' - U$  Hubbard model at half-filling: Interaction strengths in cuprate superconductors and an effective spin-only description of  $\text{La}_2\text{CuO}_4$ ,” *Phys. Rev. B* **79**, 235130 (2009).
- [55] Hong-Yu Yang, Andreas M. Läuchli, Frédéric Mila, and Kai Phillip Schmidt, “Effective Spin Model for the Spin-Liquid Phase of the Hubbard Model on the Triangular Lattice,” *Phys. Rev. Lett.* **105**, 267204 (2010).
- [56] Sandro Sorella, Yuichi Otsuka, and Seiji Yunoki, “Absence of a Spin Liquid Phase in the Hubbard Model on the Honeycomb Lattice,” *Scientific Reports* **2**, 992 EP – (2012).
- [57] Tian-Heng Han, Joel S. Helton, Shaoyan Chu, Daniel G. Nocera, Jose A. Rodriguez-Rivera, Collin Broholm, and Young S. Lee, “Fractionalized excitations in the spin-liquid state of a kagome-lattice antiferromagnet,” *Nature* **492**, 406–410 (2012).
- [58] Steven R. White and A. L. Chernyshev, “Neél Order in Square and Triangular Lattice Heisenberg Models,” *Phys. Rev. Lett.* **99**, 127004 (2007).
- [59] Wen-Jun Hu, Shou-Shu Gong, Wei Zhu, and D. N. Sheng, “Competing spin-liquid states in the spin- $\frac{1}{2}$  Heisenberg model on the triangular lattice,” *Phys. Rev. B* **92**, 140403 (2015).